

Article

Non-Iterative Coordinated Optimisation of Power–Traffic Networks Based on Equivalent Projection

Wei Dai ^{1,*}, Zhihong Zeng ¹, Cheng Wang ², Zhijie Zhang ¹, Yang Gao ¹  and Jun Xu ¹

¹ School of Electrical Engineering, Guangxi University, Nanning 530004, China;

2112392006@st.gxu.edu.cn (Z.Z.); zhijiezh@163.com (Z.Z.); 2112301084@st.gxu.edu.cn (J.X.)

² Gui'an Power Supply Bureau of Guizhou Power Grid Co., Ltd., Gui'an 550025, China; 18965167687@163.com

* Correspondence: weidai2019@163.com or weidai@gxu.edu.cn

Abstract: The exchange of sensitive information between power distribution networks (PDNs) and urban transport networks (UTNs) presents a difficulty in ensuring privacy protection. This research proposes a new collaborative operation method for a coupled system. The scheme takes into account the schedulable capacity of electric vehicle charging stations (EVCSs) and locational marginal prices (LMPs) to handle the difficulty at hand. The EVCS hosting capacity model is built and expressed as the feasible area of charging power, based on AC power flow. This model is then used to offer information on the real schedulable capacity. By incorporating the charging loads into the coupling nodes between PDNs and UTNs, the issue of coordinated operation is separated and becomes equal to the optimal problem involving charging loads. Based on this premise, the most efficient operational cost of PDNs is transformed into a comparable representation of cost information in PDNs. This representation incorporates LMP information that guides charging decisions in UTNs. The suggested collaborative scheduling methodology in UTNs utilises the collected projection information from the static traffic assignment (STA) to ensure data privacy protection and achieve non-iterative calculation. Numerical experiments are conducted to illustrate that the proposed method, which uses a smaller amount of data, achieves the same level of optimality as the coordinated optimisation.



Citation: Dai, W.; Zeng, Z.; Wang, C.; Zhang, Z.; Gao, Y.; Xu, J. Non-Iterative Coordinated Optimisation of Power–Traffic Networks Based on Equivalent Projection. *Energies* **2024**, *17*, 1899. <https://doi.org/10.3390/en17081899>

Academic Editors: Stefano Bracco, Ruixin Yang, Jinhao Meng, Qian Xiao, Zeyu Chen, Yanan Wang, Dongdong Zhao, Daniel Stroe and Ji Wu

Received: 2 February 2024

Revised: 7 April 2024

Accepted: 13 April 2024

Published: 16 April 2024



Copyright: © 2024 by the authors. Licensee MDPI, Basel, Switzerland. This article is an open access article distributed under the terms and conditions of the Creative Commons Attribution (CC BY) license (<https://creativecommons.org/licenses/by/4.0/>).

Keywords: electric vehicles (EV); coordinated optimisation; equivalent model; non-iterative; power and traffic system

1. Introduction

EVs have gained considerable international recognition due to concerns such as the oil crisis and carbon emissions. They have emerged as a prominent alternative to replace cars that run on petrol [1]. Global EV forecast research [2] predicts that the number of EVs in use globally will increase to 270 million by 2030, representing almost 14% of the total number of vehicles on the road. However, the extensive integration of electric vehicles (EVs) is expected to establish a mutually dependent relationship between PDNs and UTNs [3,4]. The travel patterns of EVs will be impacted by different road conditions, leading to changes in the spatial and temporal distribution of traffic flow. However, the charging price and queueing time at EVCSs are expected to influence the preferences of EV drivers for charging stations and, as a result, change the distribution of the electrical demand. Therefore, it is crucial to include coupling parameters in the coordination and scheduling of PTNs [5–9].

In this regard, researchers have recently focused on studying the interactions in PTNs to effectively accommodate the widespread use of EVs. Therefore, due to concerns regarding computational efficiency and data security, a substantial amount of study is focused on examining the coordination of joint flow. One specific form of research focuses on centralised optimisation by using joint modelling of PTNs and applying various acceleration strategies for computation. In the given example, a stochastic optimisation framework is developed to analyse the interconnections of PTNs in [10,11]. These interconnections include

relationships between EVs/fuel-based automobiles, charging costs, and charging power. In [12], a coordination model is proposed that is based on the generalised user equilibrium in power–traffic coupled networks. This model effectively reduces the pressure in the power distribution networks with EVs. Furthermore, a model that combines dynamic user equilibrium and that is based on [8,13,14] is introduced to accurately represent the flows in PTNs. The paper [15] presents a scheduling technique that combines the assignment of charging stations and the allocation of charging power to ensure an appropriate charging plan for each EV. In their study, the authors of [16] develop a two-stage architecture that integrates optimal pathways and active and reactive power regulation for EVs in order to minimise the cost of charging. A comprehensive model is developed in [17–19] to address the intricate relationship between EVs, the power grid, and photovoltaics. This model incorporates multiple stages and takes into account the routing and scheduling of EVs to effectively handle complex traffic scenarios. In order to address congestion in UTNs, a pricing model that incorporates both LMPs and congestion charges is proposed. This model is built on a variational inequality framework, as described in [20].

The previously described research on centralised optimisation enhances computational efficiency by integrating electricity and transportation modelling. However, due to the fact that the electricity and traffic systems are controlled by various entities with distinct information security needs, it is not feasible to implement a centralised method that requires sharing of information [21].

In addition to centralised optimisation methods, decentralised procedures that rely on limited information iteration are also crucial for coordinating scheduling in networked systems. A bi-level coordinate operation framework is built using the alternative direction method of multipliers (ADMM) in [14,22,23], considering both systemic and individual views. In [24], a decentralised collaborative pricing method is proposed which uses variational inequalities. Based on this premise, a decentralised and decoupling architecture is constructed to effectively address the issue. In order to achieve the best outcome and maintain the anonymity of information, a scheme has been developed that combines the numerous individual decisions of EVs in PTNs. This strategy involves two separate network operators and uses small data, as described in reference [25]. A decentralised approach is utilised in [26] to address the collaborative pricing model, which encompasses road tolls and charging costs.

Several academics have examined several variables that impact the process of charging EVs. As an illustration, the researchers in [27] conducted a research study to analyse the effect of charging station placements on PDNs. The failure of a charging station does not impact the charging behaviour of electric buses, as seen in [28]. In a previous study, scientists employed genetic algorithms to forecast forthcoming charging requirements for EVs and strategise the most advantageous sites for charging stations [29]. A comparison analysis was conducted in [30] to compare wireless charging with traditional charging models. The writers of [31] concentrate on long-distance transportation for EVs and devise the most efficient sites for charging stations to guarantee rapid charging capabilities. In their study, the authors of [32] used an optimisation model to determine the optimal placement of charging stations and the appropriate size of electric cars. They took into account factors such as time-of-use energy price and the behaviour of electric buses to ensure the safe and efficient operation of PTNs. In order to address the charging requirements and enhance the charging effectiveness for electric vehicle users, a dispatch model for electric vehicles is suggested in [33]. This approach employs price advice to reduce the burden on charging stations. The authors of [34] consider the unpredictability of wind power generation and optimise the charging behaviour of electric buses to efficiently utilise renewable energy resources and decrease the use of non-clean energy sources. In order to synchronise the economic dispatch in PDNs with the traffic assignment in transportation networks (TNs), a decentralised architecture is suggested to develop the most efficient charge price in [35]. In their study, the authors of [36] investigate social optimal welfare by examining the charging fees and the interactions between cooperative Charging Network Operators, mobile EVs,

and bulk power infrastructures. In addition, the authors of [37] suggest a framework that integrates pricing for charging and scheduling of power.

Using a decentralised strategy to synchronise power–traffic flows is in perfect harmony with the practical reality of their operation by two separate entities. This strategy successfully addresses the difficulties presented by restricted data sharing while guaranteeing the highest level of data privacy. However, due to the dependence on information iteration, there are several disadvantages to traditional decentralised approaches. (1) Within the domain of conventional distributed algorithms, such as Lagrangian relaxation [38], Benders decomposition [39], and generalised Benders decomposition [40], these methods may face challenges related to slow convergence or even the potential for convergence failure. (2) In order to maintain equilibrium in the coupled system, the increased frequency of information exchange will place a greater strain on communication resources. (3) The increasing number of distribution networks and transportation systems will result in a significant increase in the iteration count [41].

This study focuses on implementing the analogous projection approach to address the previously mentioned limitations in PTNs. The strategy, initially presented in [42], aims to achieve system reduction and has been proven to provide the same level of optimality as the primal model. Moreover, the technique is utilised in [43] to efficiently synchronise the optimisation process between the transmission and distribution of electrical power networks. In [44], the authors successfully characterised the charging power area of EVCS using this method. However, they have not yet included the projection of optimal cost information in PDNs.

The aforementioned approaches are specifically employed to address the interconnections of power systems. However, the interactions of traffic systems are considerably more complex, involving factors such as the unpredictability of individual behaviour of EVs and the multitude of road pathways. In order to achieve this goal, this study aims to create a thorough modelling framework using network equivalent projection that includes the schedulable capacity of EVCSs and LMPs. This framework will enable effective interaction and allow for reaching the optimal operating point with minimal information in PTNs. This paper presents the following primary contributions:

1. A novel non-iterative coordinated optimisation method for PTNs is created using network equivalent projection. The coupled networks incorporate the schedulable capacity of EVCSs and dynamic LMPs at charging stations, and map this information into the feasible region of boundary information for PDNs. Implementing this suggested methodology can safeguard data confidentiality without the need to share sensitive information.

2. A technique is introduced to map the optimal cost function in the PDN. The segmented cost function of the PDNs is produced by specifically addressing the economic dispatch model and the Karush–Kuhn–Tucker (KKT) conditions. The original linked model of the PTN is substituted with integrated equivalent restrictions and segmented cost functions incorporating the traffic model. This proposed approach will guarantee manageable computation in the PTN.

The subsequent sections of this work are structured in the following manner. The coordinated optimisation model of the PTNs is established in Section 2. Section 3 introduces a decoupled model of the PTNs based on the feasible region of the PDNs. This model is created using network equivalent projection and takes into account the schedulable capacity of EVCS and LMPs. A unique optimal cost mapping methodology for the PDN is devised in Section 4. A case study is conducted to validate the effectiveness and advantages of the suggested approach outlined in Section 5. The conclusions are presented in Section 6.

2. Power–Traffic Coupled Model Equation

2.1. Interaction of the Coupled PTNs

The interconnection between PDNs and UTNs is strongly interconnected as a result of EVs. The EVCS recharge facilities facilitate the interplay between the flow of power and the flow of traffic. Figure 1 illustrates the operational framework of the interconnected

power–traffic system. Pricing methods employed by electricity and transportation system organisations have an impact on the driving and charging decisions made by vehicle users. EV drivers choose their driving routes and charging stations based on price signals that are limited by the PDN and road conditions, with the goal of minimising their travel expenses.

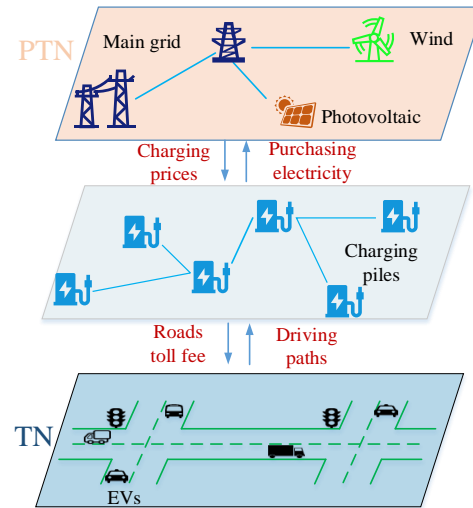


Figure 1. Operation framework of coupled power-traffic system.

2.2. A Traffic Model for the Travel Characteristics of Vehicles

From a graph theory standpoint, the fundamental components of the UTN are examined, with crossings being considered as nodes and road segments as connections. Moreover, the structure of the UTN is represented as (V, A) , where V and A are collections of sequentially numbered intersections and road segments, respectively. An O-D pair represents the route used by electric vehicles (EVs) from a starting point to a destination, which indicates the traffic demand. Based on this premise, the traffic assignment problem is transformed into the calculation of traffic flow on various paths in a UTN, with each origin–destination pair specified.

An investigation is conducted to examine the travel characteristics of various EVs in order to meet the charging needs of EVs.

2.2.1. Road Congestion Analysis Based on Various Types of EVs

The structure of the transportation network consists of interconnected links and nodes. The links symbolise several paths or routes, while the nodes indicate the starting points, ending points, and points where different paths overlap. In order to model the travel patterns of EVs, the links in the UTN will be split into three equal segments: charging links, ordinary links, and bypass links [6].

1. Charging links with EVCSs

The travel time of EVs on a charging link is determined by the combined factors of charging time and queueing time. Hence, the improved Davidson function considering queueing theory is employed to quantify the travel time $t_a^c(x_a)$ of charging EVs, i.e.,

$$t_a^c(x_a) = t_a^{FCS} \left[1 + J \left(\frac{x_a}{c_a^{FCS} - x_a} \right) \right], \quad \forall a \in T^C(A) \quad (1)$$

where t_a^{FCS} represents the free traveling time in the charging oracle, i.e., the charging time. x_a is the traffic flow of the a -th link. c_a^{FCS} is the traffic capacity of the a -th charging segment. J represents the parameter controlling the shape of the congestion function in the charging segment. $T^C(A)$ denotes the set of all charging links in UTNs.

2. Regular links without EVCSs

The widely used Bureau of Public Road (BPR) function is adopted in this work to represent the time spent on a regular link, i.e.,

$$t_a^R(x_a) = t_a^0 \left[1 + 0.15 \left(\frac{x_a}{c_a} \right)^4 \right], \quad \forall a \in T^R(A) \quad (2)$$

where t_a^0 is the free traveling time of the a -th link. c_a is the traffic capacity of the a -th link. $T^R(A)$ denotes the set of all regular links in UTNs.

3. Bypass links

A bypass link denotes a road segment with an EVCS where EVs skip and continue to drive without interruption. Due to the short length of the bypass oracle, it can be assumed that the travel time through this link is negligible and approximated as zero, i.e.,

$$t_a^b(x_a) = 0, a \in T^B(A) \quad (3)$$

where $T^B(A)$ is the set of all bypass links. $T(A)$ is the set of all links in UTNs: $T^C(A) \cup T^R(A) \cup T^B(A) = T(A)$.

2.2.2. Modelling the Costs of Vehicles Based on Different Driving Behaviours

Based on the above different types of congestion in UTNs, the travel cost functions of different paths are established for various transportation participants. For EVs with charging, a feasible path must include at least a charging station. The set of feasible paths K_{od} is expressed as

$$K_{od} = K_{od}^C \cup K_{od}^R \quad (4)$$

where K_{od}^C , K_{od}^R denote feasible path sets for EVs with recharging and regular vehicles, respectively.

1. The travel costs of EVs with charging

To estimate the travel cost of EVs with recharging, it is essential to consider three key components: the monetary value of time spent driving on regular links, the queueing time in EVCSs, and the charging cost. Accordingly, the travel time t_k^{od} and cost c_k^{od} of an EV with charging on the feasible path k -th are, respectively, represented by

$$t_k^{od} = \sum_{a \in T^C(A)} t_a^c(x_a) \delta_{a,k}^{od} + \sum_{a \in T^R(A)} t_a^c(x_a) \delta_{a,k}^{od}, \quad \forall k \in K_{od}^C, \forall (o, d) \quad (5)$$

$$c_k^{od} = \omega t_k^{od} + \sum_{a \in T^C(A)} \left(\lambda_a^j P_{FCS} t_a^{FCS} \right) \delta_{a,k}^{od}, \quad \forall k \in K_{od}^C, \forall (o, d) \quad (6)$$

where t_k^{od} and c_k^{od} denote the travel time and cost of a feasible path k between the O-D pair, respectively. ω is the unit travel cost coefficient. λ_a^j represents the charging price in EVCS a supplied by node j in a PDN. P_{FCS} is the charging power of EVs.

2. The travel costs of regular EVs

The total cost of regular vehicles is calculated by factoring in only the monetary value of time spent driving on regular links, i.e.,

$$t_k^{od} = \sum_{a \in T^R(A)} t_a^R(x_a) \delta_{a,k}^{od}, \quad \forall k \in K_{od}^R, \forall (o, d) \quad (7)$$

$$c_k^{od} = \omega t_k^{od}, \quad \forall k \in K_{od}^R, \forall (o, d) \quad (8)$$

2.2.3. A Traffic Model Based on User Equilibrium

As the charging behaviours of EV users affect the feasible path set and cause divergence from the path choices of non-charging users, it is vital to express the user equilibrium (UE)

condition more explicitly. On this basis, an EV charging equilibrium model originating from [6] is utilised to characterise the equilibrium state in the UTN, i.e.,

$$\min \sum_{t \in T(T)} \left(\sum_{a \in T^R(A)} \int_0^{x_a} \omega t_a^R(\theta) d\theta + \sum_{a \in T^C(A)} \int_0^{x_a} \omega t_a^C(\theta) d\theta \right) \quad (9)$$

$$f_{k,t}^{od} \geq 0, \forall t \in T, \forall k \in K^{od}, \forall od \in (O, D) \quad (10)$$

$$r_t^{od} = \sum_{k \in K_{od}} \frac{f_{k,t}^{od} t_{k,t}^{od}}{\tau_{RF}}, \forall t \in T, \forall k \in K \quad (11)$$

$$q_{od,t}^{mod} = q_{od,t} + \frac{1}{2} r_{t-1}^{od} - \frac{1}{2} r_t^{od}, \forall t \in T, \forall od \in (O, D) \quad (12)$$

$$\sum_{k \in K_{od}^C} f_{k,t}^{od} = \mu q_{od,t}^{mod}, \forall t \in T, \forall od \in (O, D) \quad (13)$$

$$\sum_{k \in K_{od}^R} f_{k,t}^{od} = (1 - \mu) q_{od,t}^{mod}, \forall t \in T, \forall od \in (O, D) \quad (14)$$

$$x_{a,t} = \sum_{o \in O} \sum_{d \in D} \sum_{k \in K_{od}} f_{k,t}^{od} \delta_{a,k}^{od}, \forall t \in T, \forall a \in T(A) \quad (15)$$

where f_k^{od} is the traffic flow on the k -th path connecting the O-D pair. q_{od} represents the total travel demand between the O-D pair. $\delta_{a,k}^{od}$ is a binary variable that represents the relationship between link a and path k connecting the O-D pair when $\delta_{a,k}^{od} = 0$ if link a is included in path k , and $\delta_{a,k}^{od} = 1$ otherwise. μ denotes the ratio of the number of EVs with charging to the total transportation demand.

In the given model, Equation (9) represents the objective of minimising the total cost of travel for traffic users. Equation (10) ensures that the traffic flow remains non-negative. Equations (11) and (12) describe the temporal relationship between traffic flow by incorporating the remaining flow from path k in the previous period into the traffic demand in the next period. Equations (13) and (14) represent the balance between traffic demand and path flow for traffic users on the feasible path k . Equation (15) states that the traffic flow in link a is equal to the sum of the traffic flows on all paths passing through this oracle.

2.3. Modelling of the Optimal Power Flow in the PDN

A radial PDN adopted in this part is represented by a directed graph (N, L) , where N denotes the set of nodes and L means the set of branches. The initial node designated as $\{1\}$ is connected to the transmission power grid and purchases electricity directly from the main grid. The other nodes can be numbered sequentially as $N^+ = \{2, \dots, n\}$, and so on. $(i, j) \in L$ corresponds to a branch from node i to node j . The sets N_{FCS} denote the collection of nodes that are connected to the EVCS. $\Phi(i)$ refers to the set of sub-nodes that are connected to node i , while $\Pi(j)$ means the set of nodes that stem from node j . The optimal power flow is regarded as Equations (16)–(24), in which the subscript t represents the time interval.

$$\min \sum_{t \in T} \left(\underbrace{\sum_{j \in N^+} \left(a_j (P_{DG,jt})^2 + b_j P_{DG,jt} \right)}_i + \lambda_{MAIN,t} \underbrace{\sum_{j \in \Phi(1)} P_{1jt}}_{ii} \right) \quad (16)$$

s.t.

$$\sum_{i=1}^{Ng} P_{Gi,t} - \sum_{i=1}^{Ne} P_{EVCSi,t} = P_{loss,t} + P_{L,t}, \forall t \in T \quad (17)$$

$$P_{i,t} - V_{i,t} \sum_{j=1} V_{j,t} \left(\frac{\cos \delta_{ij,t}}{r_{ij}} + \frac{\sin \delta_{ij,t}}{x_{ij}} \right) = 0, \forall t \in T \quad (18)$$

$$Q_{i,t} - V_{i,t} \sum_{j=1} V_{j,t} \left(\frac{\sin \delta_{ij,t}}{r_{ij}} - \frac{\cos \delta_{ij,t}}{x_{ij}} \right) = 0, \forall t \in T \quad (19)$$

$$P_{i,t}^2 + Q_{i,t}^2 \leq (S_{ij,t}^{MAX})^2, \forall t \in T \quad (20)$$

$$0 \leq P_{DG,j,t} \leq P_{DG,j}^{\max}, \forall j \in N^+ \quad \forall t \in T \quad (21)$$

$$0 \leq Q_{DG,j,t} \leq Q_{DG,j}^{\max}, \forall j \in N^+ \quad \forall t \in T \quad (22)$$

$$V_{\min} \leq V_{j,t} \leq V_{\max}, \forall j \in N \quad \forall t \in T \quad (23)$$

$$P_{EVCS}^{\min} \leq P_{EVCSi,t} \leq P_{EVCS}^{\max} \quad \forall t \in T \quad (24)$$

where $P_{1,j,t}$ is the power purchased from the main grid. T denotes the entire scheduling period. a_j and b_j represent the cost coefficient of the controllable generations connected to node j in the PDN. $P_{DG,j}$ and $Q_{DG,j}$ refer to the active and reactive power output of the controllable generation at node j . λ_{MAIN} represents the purchasing electricity price from the main grid. P_i and Q_i denote the injective active and reactive power at node i . P_{ij} and Q_{ij} refer to the active and reactive power transmitted in the branch (i,j) , respectively. r_{ij} and x_{ij} represent the equivalent resistance and reactance of the branch (i,j) . V_j denotes the voltage magnitude at node j . δ_j is the voltage phase angle at node j . $P_{L,j}$ and $P_{loss,t}$ are conventional active loads and loss power at node j , respectively. $P_{EVCS,j}$ represent the charging loads of EVCSs located at node j . $P_{DG,j}^{\max}$ and $Q_{DG,j}^{\max}$ represent, respectively, the upper bound of the distributed units' active and reactive power output. V_{max} and V_{min} are the upper and lower bounds of the nodal voltage magnitudes. P_{EVCS}^{\max} and P_{EVCS}^{\min} represent the active power limits in the EVCSs, respectively.

The objective function of Equation (16) represents the minimum operational cost of the PDN, including (i) the generation cost of controllable distributed generation units and (ii) the purchase cost of electricity from the main grid. Equation (17) denotes the active power balance of the PDN. Equations (18) and (19) denote the power flow balance of the PDN. Equation (20) represents the active and reactive power transmission limits of branches. Equations (21) and (22) denote controllable generation capacity in the PDN. Equation (23) represents the nodal voltage magnitude bounds. Equation (24) is the capacity limit of EVCSs.

The power flow balance constraints (18) and (19) can be expressed using the linearization derivation from [45] in the following manner:

$$P_{i,t} \approx \sum_{j=1}^n \frac{V_{j,t}}{r_{ij}} - \sum_{j=1}^n \frac{\delta_{j,t}}{x_{ij}}, \forall t \in T \quad (25)$$

$$Q_{i,t} \approx -\sum_{j=1}^n \frac{V_{j,t}}{x_{ij}} - \sum_{j=1}^n \frac{\delta_{j,t}}{r_{ij}}, \forall t \in T \quad (26)$$

We employ the linearization method based on polygon approximation in [46] to address the branch transmission limitations. According to Equation (20), it is evident that there are many power circles being considered. Thus, it is capable of approximating the

forementioned power circles by using polygons that have a limited number of edges. Thus, Equation (20) can be converted into:

$$\bar{P}_{ij,t}P_{ij,t} + \bar{Q}_{ij,t}Q_{ij,t} \leq \left(S_{ij,t}^{\max}\right)^2, \forall t \in T \tag{27}$$

$$\bar{P}_{ij,t} = \cos\left[\left(p - \frac{E+4}{4}\right)\frac{2\pi}{E}\right], \forall p \in \left[1, 2, \dots, \frac{E}{2}\right], \forall t \in T \tag{28}$$

$$\bar{Q}_{ij,t} = \sin\left[\left(p - \frac{E+4}{4}\right)\frac{2\pi}{E}\right], \forall p \in \left[1, 2, \dots, \frac{E}{2}\right], \forall t \in T \tag{29}$$

where E represents the number of edges of the polygon approximating the power circles. The value of E can be chosen to be between 8 and 20, considering the trade-off between computational efficiency and accuracy. After evaluating the relationship between efficiency and precision, an inscribed regular dodecagon (i.e., a polygon with twelve edges) is opted to replace the power circles.

2.4. Modelling of the Coupled PTN

This section examines the interconnected boundary between the power and transportation systems, specifically focusing on the independent operation models for the UTN and the PDN mentioned earlier. The goal is to understand the relationship between the boundary information of these two systems. To achieve this, a coordinated scheduling model for the power-traffic coupling system is developed. More precisely, the interaction in a PTN occurs when EVs transfer energy by charging over the links connecting to the PDN for additional electrical power. Thus, in the PTN, the boundary information of the UTN pertains to the traffic flow of EVs entering the charging stations, while the boundary information on the PDN corresponds to the charging load of the EVCS. The correlation between the charging load linked to the PTN node j and the traffic flow in the UTN is represented as:

$$P_{FCS,j} = P_{FCS} \sum_{o \in O} \sum_{d \in D} \sum_{k \in K_{od}^C} f_k^{od} \delta_{a,k}^{od}, \forall a \in T^C(A), j \in N_{FCS} \tag{30}$$

The coordinated scheduling in the PTN is aimed at the minimum social cost, i.e.,

$$\min \sum_{a \in T^R(A)} \int_0^{x_a} \omega t_a^R(\theta) d\theta + \sum_{a \in T^C(A)} \int_0^{x_a} \omega t_a^C(\theta) d\theta + \sum_{t \in T} \left(\sum_{i \in N^+} (a_j(P_{DG,jt})^2 + b_j P_{DG,jt}) + \lambda_{\text{MAIN}} \sum_{j \in \Phi(1)} P_{1j,t} \right) \tag{31}$$

s.t.

$$\begin{cases} (10) - (15) \\ (17), (21) - (29) \end{cases} \tag{32}$$

3. Decoupled Model of the PTN Based on the Feasible Region of the PDN

Definition 1 (schedulable capacity (SC)): During the EV charging process, the PDN establishes a zone that includes all the possible operating locations of the charging loads. This region ensures stability and security by meeting the restrictions specified in (35).

To facilitate the understanding of the model derivation, a concise representation of the PTN, comprising Equations (31) and (32), is provided.

$$\min \sum_t \left(C_{PDN,t}(\mathbf{y}_{PDN,t}) + C_{UTN,t}(\mathbf{y}_{UTN,t}^a) \right) \tag{33}$$

$$\text{s.t.} \begin{cases} h_{PDN,t}^{eq}(\mathbf{y}_{PDN,t}, \mathbf{u}_t, P_t^{EVC}) = 0 \\ h_{PDN,t}^{ineq}(\mathbf{y}_{PDN,t}, \mathbf{u}_t, P_t^{EVC}) \leq 0 \end{cases} \tag{34}$$

$$g_{UTN,t}(\mathbf{y}_{UTN,t}^a, f_{k,t}^{od}) \leq 0 \quad (35)$$

$$\mathbf{A}_{CPT} P_t^{EVC} + \mathbf{B}_{CPT} \mathbf{y}_{UTN,t}^a = \mathbf{c}_{CPT,t} \quad (36)$$

The constraints of Equation (34) denote the sets formed by the equality Equations (17), (25) and (26), and inequality constraints Equations (21)–(24) and (27)–(29), respectively. The constraints of Equation (35) denote the constraint sets formed by the UTN in Equations (10)–(15). The $C_{PDN,t}$ denotes the operational cost function of the PDN. $\mathbf{y}_{PDN,t}$ is the power vector injected from controllable generators and the main grid. \mathbf{u} represents the vector of the state variable in the PDN. P_t^{EVC} is the EV maximum charging power from the PDN, which comprises the charging load and the available charging power. $C_{UTN,t}$ is the cost function of the UTN. $\mathbf{y}_{UTN,t}^a$ is a vector composed of the column vectors traffic flow x_a and time t_a , i.e., $\mathbf{y}_{UTN,t}^a = [x_a, t_a]$. \mathbf{A}_{CPT} , \mathbf{B}_{CPT} , and \mathbf{c}_{CPT} represent coefficient vectors corresponding to the PDN and the UTN in Equation (30), respectively. P_{EVC} is the charging power of EVCS.

The polyhedral space Ω_{SC}^{pri} formed by the constraint of Equation (34) is denoted as follows, where the subscript t is neglected for simplicity:

$$\Omega_{SC}^{pri} = \left\{ (\mathbf{y}_{PDN}, P^{EVC}) \in R^m \times R^n \left| \begin{array}{l} h_{PDN}^{eq}(\mathbf{y}_{PDN}, \mathbf{u}, P^{EVC}) = 0 \\ h_{PDN}^{ineq}(\mathbf{y}_{PDN}, \mathbf{u}, P^{EVC}) \leq 0 \end{array} \right. \right\} \quad (37)$$

where m and n denote the dimensions.

According to definition 1, it is shown that the schedulable capacity is interpreted as a projection from the constraints of space $(\mathbf{y}_{PDN}, \mathbf{u}, P^{EVC})$ to P^{EVC} in the PDN. The projection area Ω_{SC}^{map} is stated as

$$\Omega_{SC}^{map} = \left\{ (P^{EVC}) \in R^n \mid \exists \mathbf{y}_{PDN}, (\mathbf{y}_{PDN}, \mathbf{u}, P^{EVC}) \in \Omega_{SC}^{pri} \right\} \quad (38)$$

where Ω_{SC}^{map} describes the range of EV charging loads accommodated by the PDN at any period t without violating safety operation constraints, as shown in Equation (34).

This polyhedron, i.e., the boundary information feasibility region, is expressed as:

$$\Omega_{EVC}^{ap} = \left\{ \mathbf{A}_{EV} P_k^{EVC} \leq \boldsymbol{\beta}_{EV} \right\} \quad (39)$$

where \mathbf{A}_{EV} is the coefficient matrix for different stress directions; and $\boldsymbol{\beta}_{EV}$ is a coefficient vector that describes the boundary of the EVSC. The dimensions of \mathbf{A}_{EV} and $\boldsymbol{\beta}_{EV}$ correspond to the number of boundary points characterising the EVSC. Each determined boundary point leads to a set of constraints.

Figure 2 presents the coordinated operation framework of the coupled power–traffic system. The equivalent projection model of the PTN is expressed as:

$$\min(C_{PDN}(P_k^{EVC}) + C_{UTN}(\mathbf{y}_{UTN}^a)) \quad (40)$$

$$\mathbf{A}_{EV} P_k^{EVC} \leq \boldsymbol{\beta}_{EV} \quad (41)$$

$$g_{UTN}(\mathbf{y}_{UTN}^a, f_k^{od}) \leq 0 \quad (42)$$

$$\mathbf{A}_{CPT} P_k^{EVC} + \mathbf{B}_{CPT} \mathbf{y}_{UTN}^a = \mathbf{c}_{CPT} \quad (43)$$

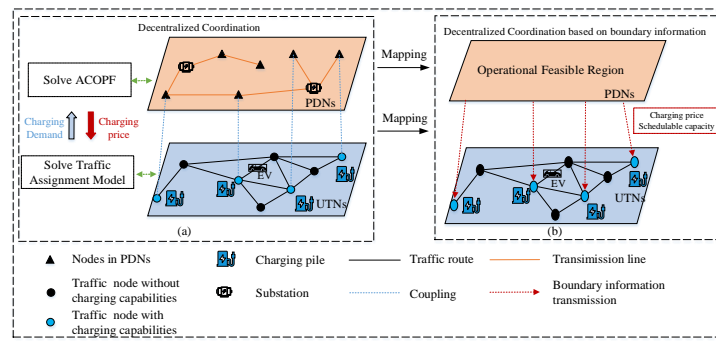


Figure 2. Coordinated operation framework of the coupled power–traffic system.

4. Mapping Optimal Costs of the PDNs

When it comes to connections including boundary EVCSs, the PTN aims to optimise the power and traffic flows. From the perspective of the PDN, charging stations are classified as variable loads since they consume electrical energy from the grid. Alternatively, when considering the transportation network, these stations can be seen as virtual sources that provide electric power to cars. The fundamental coupled model in the PTN is reconstructed and expressed as a result of boundary charging power.

$$\begin{aligned}
 & \min C_{PDN}(\mathbf{y}_{PDN}) + C_{UTN}(\mathbf{y}_{UTN}^a) \\
 \text{s.t.} \quad & \begin{cases} h_{PDN}^{eq}(\mathbf{y}_{PDN}, u, P^{EVC}) = 0 \\ h_{PDN}^{ineq}(\mathbf{y}_{PDN}, u, P^{EVC}) \leq 0 \\ g_{UTN}(\mathbf{y}_{UTN}^a, f_k^{od}) \leq 0 \end{cases} \\
 & A_{PDN}\mathbf{y}_{PDN} + D_{PDN}P_k^{EVC} = c_{PDN} \\
 & B_{UTN}\mathbf{y}_{UTN}^a + D_{UTN}P_k^{EVC} = c_{UTN}
 \end{aligned} \tag{44}$$

where vector D denotes the charging power at a charging station.

The equivalent model consisting of Equations (33)–(36) implies that each PDN and the UTN perform optimal social welfare individually with limited data exchange. Hence, the model of the PDN at the time t is reformulated and expressed as

$$\begin{aligned}
 & f_{PDN}(P_k^{EVC}) = \min C_{PDN}(\mathbf{y}_{PDN}) \\
 \text{s.t.} \quad & \begin{cases} h_{PDN}^{eq}(\mathbf{y}_{PDN}, u, P^{EVC}) = 0 \\ h_{PDN}^{ineq}(\mathbf{y}_{PDN}, u, P^{EVC}) \leq 0 \\ A_{PDN}\mathbf{y}_{PDN} + D_{PDN}P_k^{EVC} = c_{PDN} \end{cases}
 \end{aligned} \tag{45}$$

where the objective function of $f_{PDN}(P_k^{EVC})$ means the optimal social cost of the PDN related to the boundary charging power P_k^{EVC} .

It has been demonstrated that there is an equivalence in optimality between the joint optimisation Equations (45) and (46), i.e.,

$$\begin{aligned}
 & \min (f_{PDN}(P_k^{EVC}) + C_{UTN}(\mathbf{y}_{UTN}^a)) \\
 \text{s.t.} \quad & \begin{cases} g_{UTN}(\mathbf{y}_{UTN}^a, f_k^{od}) \leq 0 \\ B_{UTN}\mathbf{y}_{UTN}^a + D_{UTN}P_k^{EVC} = c_{UTN} \end{cases}
 \end{aligned} \tag{46}$$

From the modified model (see Equation (46)), it is crucial to derive the specific form of the function $C_{PDN}(D_{PDN})$. According to Equation (16), the form of the objective function in PDN is quadratic, which is converted and stated as:

$$F_{PDN}(P_{DG}) = \frac{1}{2}P_{DG}A_{Re}^T P_{DG} + B_{Re}^T P_{DG} + \lambda_{MAIN}P_1 \tag{47}$$

where vector P_{DG} and P_1 denote all $P_{DG,j}$ and P_{1j} , respectively. The syntax $A_{Re}^T = (a_1, \dots, a_i)^T$ and $B_{Re}^T = (b_1, \dots, b_i)^T$ are utilised to concatenate column vectors with the cost coefficient of the controllable generators.

With the charging power given, the optimal objective in Equation (47) is computed, and the solution corresponds to an optimal value, where the constraints are categorised into active and inactive ones. These constraints divided are rewritten, i.e.,

$$(A_{PDN})_a P_{DG} + (D_{PDN})_a P^{EVC} = (c_{PDN})_a \tag{48}$$

$$(A_{PDN})_{ina} P_{DG} + (D_{PDN})_{ina} P^{EVC} \leq (c_{PDN})_{ina} \tag{49}$$

where Equation (48) means the active constraints, denoted by subscript a . Additionally, Equation (49) is the inactive constraints with subscript ina .

From the perspective of optimisation theory, the optimal solution of the model is not affected by inactive constraints. Hence, Equation (46) is modified equivalently, i.e.,

$$\begin{aligned} & \min F_{PDN}(P_{DG}) \\ & \text{s.t. } (A_{PDN})_a P_{DG} + (D_{PDN})_a P^{EVC} = (c_{PDN})_a \end{aligned} \tag{50}$$

The Lagrange function is expressed as:

$$L(P_{DG}, \mu) = \frac{1}{2} P_{DG} A_{Re}^T P_{DG} + B_{Re}^T P_{DG} + \lambda_{MAIN} P_1 + \eta^T \left((A_{PDN})_a P_{DG} + (D_{PDN})_a P^{EVC} - (c_{PDN})_a \right) \tag{51}$$

By applying complementary slackness conditions of KKT theory,

$$\frac{\partial L(P_{DG}, \mu)}{\partial P_{DG}} = A_{Re}^T P_{DG} + B_{Re}^T + (A_{PDN})_a^T \mu = 0 \tag{52}$$

Simultaneously ensuring the satisfaction of the active constraints of Equation (49) gives:

$$\begin{pmatrix} A_{Re}^T & (A_{PDN})_a^T \\ (A_{PDN})_a & 0 \end{pmatrix} \begin{pmatrix} P_{DG} \\ \eta \end{pmatrix} = \begin{pmatrix} -B_{Re}^T \\ (c_{PDN})_a - (D_{PDN})_a P^{EVC} \end{pmatrix} \tag{53}$$

By solving Equation (53), the values P_{DG} , η are

$$\begin{cases} P_{DG} = (A_{PDN})_a^{-1} \left((c_{PDN})_a - (D_{PDN})_a P^{EVC} \right) \\ \eta = -A_{Re}^T \left((A_{PDN})_a (A_{PDN})_a^T \right)^{-1} \left((c_{PDN})_a - (D_{PDN})_a P^{EVC} \right) \\ \quad - \left((A_{PDN})_a^T \right)^{-1} B_{Re}^T \end{cases} \tag{54}$$

There exists a linear relationship between the active power from the main grid and the charging power (i.e., P^{EVC}). It is shown that $f_{PDN}(P^{EVC})$ is a quadratic function.

Nonetheless, the above derivation process should be performed in the neighbour interval of the given charging power value (i.e., \hat{P}^{EVC}), and the active and inactive constraints in Equations (49) and (50) remain unchanged. Hence, it is essential to analyse the conditions affecting the neighbour interval.

Condition 1: Lagrange multipliers η remain non-negative, ensuring that the inequality constraints of the problem Equation (49) are satisfied, i.e.,

$$\eta \geq 0 \tag{55}$$

Condition 2: To guarantee the feasibility of Equation (47), the solution of Equation (51) must satisfy the inactive constraints of Equation (49).

To obtain the optimal cost function of the PDN under the feasible region, a piecewise approach is proposed. Specifically, based on the constraints set in Equation (46), the upper and lower bounds of the charging power (i.e., P^{EVC}) are expressed as

$$\text{s.t. } \begin{cases} \underline{P}^{EVC} = \min P^{EVC} \\ \overline{P}^{EVC} = \max P^{EVC} \\ h_{PDN}^{eq}(\mathbf{y}_{PDN}, u, P^{EVC}) = 0 \\ h_{PDN}^{ineq}(\mathbf{y}_{PDN}, u, P^{EVC}) \leq 0 \\ \mathbf{A}_{PDN}\mathbf{y}_{PDN} + \mathbf{D}_{PDN}P^{EVC} = \mathbf{c}_{PDN} \end{cases} \quad (56)$$

where $\underline{P}^{EVC}, \overline{P}^{EVC}$ denote the upper and lower bounds of the charging power, respectively.

After conducting the analysis mentioned above, it is clear that the deduction can only be valid within a neighbour interval. To achieve this, the feasible region interval $[\underline{P}^{EVC}, \overline{P}^{EVC}]$ is divided into multiple sub-intervals, with each sub-interval determined by conditions 1 and 2. One significant advantage of determining the interval width based on active and inactive constraints is the ability to enumerate all sub-intervals, which satisfies the following constraint, i.e.,

$$d_{PDN}^{m-1} \leq d_{PDN}^m \quad (57)$$

where the m -th upper bound denotes d_{PDN}^m , and the m -th sub-interval is expressed as $[d_{PDN}^{m-1}, d_{PDN}^m]$.

As the exploration of sub-intervals continues, the right endpoint d_{PDN}^m of the sub-interval is equal to the upper bound \overline{P}^{EVC} of the feasible region, which is used as a stopping criterion to express the end of the exploration process. The specific form of the optimal cost in the PDN is expressed as

$$f_{PDN}(P^{EVC}) = \sum_{m \in M} f_{PDN}^m(d_{PDN}^m) \quad (58)$$

where M is the overall count of sub-intervals. $f_{PDN}^m(d_{PDN}^m)$ denotes the optimal cost of the m -th sub-interval in the PDN.

According to the definition of LMPs, the charging price is

$$LMP = \frac{\partial f_{PDN}(P^{EVC})}{\partial P^{EVC}} \quad (59)$$

5. Case Study

5.1. Basic Settings

This part develops a connected electric-transportation system for the purpose of conducting simulation analysis. Figure 3 displays the topology of the traffic network. There are a total of six EVCSs and four distinct types of highways in both the outer and inner loops. The trip demand, free travel time, and traffic capacity for each origin-destination pair (O-D pair) are previously known, and specific parameter configurations are supplied in Tables 1 and 2. The EVs have an average charging power of 50 kW, and it is estimated that the average charging time is 30 min. The journey time is valued at USD 10 per hour.

Table 1. Link parameters of roads in the 12-node transportation network.

Road	Type 1	Type 2	Type 3	Type 4	EVCS
$c_a(p.u)$	100	100	80	60	15
$t_a^0(min)$	5	8	5	7	20

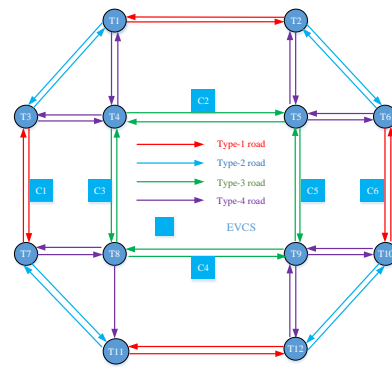


Figure 3. Topology of the UTN.

Table 2. O-D pairs and trip rates of $t = 1$ (in p.u.).

O-D Pair	q_g^{rs}	q_e^{rs}
T1–T6	9	1
T1–T10	36	4
T1–T11	18	2
T1–T12	27	3
T3–T6	9	1
T3–T10	27	3
T3–T11	18	2
T3–T12	27	3

Figure 4 displays the configuration of the updated IEEE 33-bus system. Node 1 was linked to the primary power network for the purpose of procuring electricity. Nodes 8, 15, and 31 were linked to electric vehicle (EV) charging stations, which have a maximum charging capacity of 400 kW. Controllable generations with voltage regulation facilities were connected to nodes 18 and 33. The scheduling period was fixed at 24 h. The simulations in this part were performed on the lenovo Y9000P laptop equipped with an AMD Ryzen 7 5800H processor with Radeon Graphics, running at a clock speed of 3.20 GHz, and 16 GB of RAM. The models were solved using MATLAB R2021b and YALMIP toolboxes, with the solvers IBM CPLEX 12.8 and IPOPT.

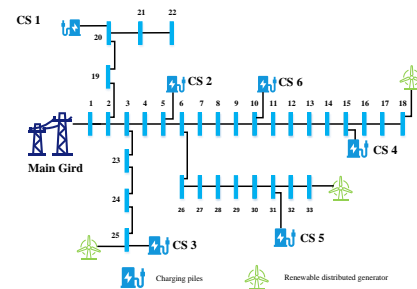


Figure 4. Topology of the PDN.

In order to assess the efficacy of the suggested method utilising equivalent projection, three specific scenarios were constructed for thorough investigation.

M1: The independent scheduling operation of the power–traffic network without coupling.

M2: The coordinated scheduling operation of the power–traffic network with the centralised method.

M3: The coordinated scheduling operation of the power–traffic network with equivalent projection.

5.2. Analysis Discussion

The cost of the power–traffic linked system is clearly lower than operating the power grid and traffic network separately, as shown in Figure 5. Furthermore, as the adoption of EVs continues to grow, the disparity between the overall cost of the integrated power–traffic system and the individual operation managed by M1 in the power–traffic networks becomes more pronounced. The effectiveness of coupled system scheduling in significantly reducing operational expenses is proved when compared to standalone scheduling. Furthermore, the overall expense of the power–traffic coupled network with M2 is equal to the one computed by M3 (refer to Figure 5). This suggests that by employing the cost function of the PDNs, the cost coupling in PTNs may be correctly aligned.

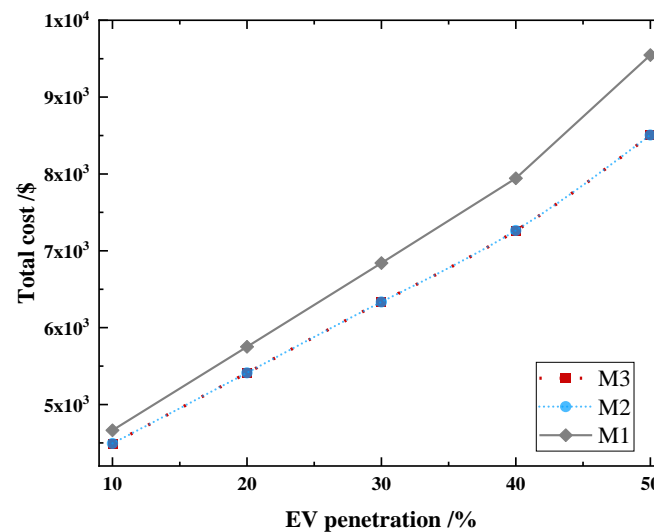


Figure 5. Total costs of the PTNs under different EV penetration levels.

Figure 6 examines the charging frequency of EVs at charging stations within the transportation network during the peak time ($t = 10$). In a scenario where there is a 10% penetration rate, the scheduling using M1 does not require a direct connection between the UTN and the PDN. Due to their higher capacity and lower waiting times, the majority of EVs prefer to charge at EVCS 2 and 6. The number of charging vehicles at Station 2 and Station 6 is 4.95 and 4.68, respectively, which together make up nearly 75% of the total charging vehicle count. The independent scheduling of EV charging results in uneven distribution of EV traffic flow, leading to high saturation levels at EVCS 2 and 6. Additionally, the paucity of charging stations at Stations 1, 4, and 5 exacerbates this issue. Unlike the uncoordinated scheduling, the coordinated scheduling of the power–traffic network efficiently reduces the concentrated distribution of EV traffic flow, leading to a more balanced traffic flow distribution and an improved utilisation rate for charging stations. Furthermore, it is important to mention that, regardless of the different levels of EV adoption, the number of times EVs need to be charged at charging stations, as calculated using M2 and M3, is consistent with the results obtained from the centralised coordinated scheduling of the power–traffic system.

Significantly, if the penetration rate falls below 40%, the aggregate demand for electric vehicles remains relatively modest, which does not pose any risk to the secure functioning limits of the power distribution networks. Nevertheless, the scenario will undergo a transformation once the EV adoption rate surpasses 40%. Figure 7 illustrates the voltage magnitudes of the PDNs when the EV penetration rate is 50%. Through a thorough examination of Figures 7 and 8, it becomes evident that EVs have a tendency to gather or cluster near EVCSs 1 and 4. Consequently, the voltage magnitudes at nodes 15 and 16 in the distribution network decrease to 0.9186 and 0.9190, respectively, indicating voltage violations in the power grid. The increased traffic in the road segments where charging

stations are situated results in higher impact loads on the distribution grid nodes that are connected to the charging stations.

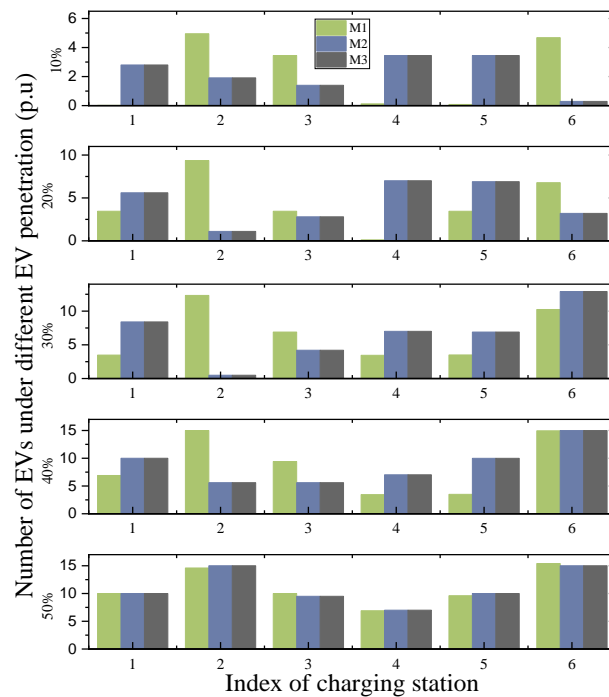


Figure 6. Distribution of EV charging numbers among EVCSs under different EV penetration levels.

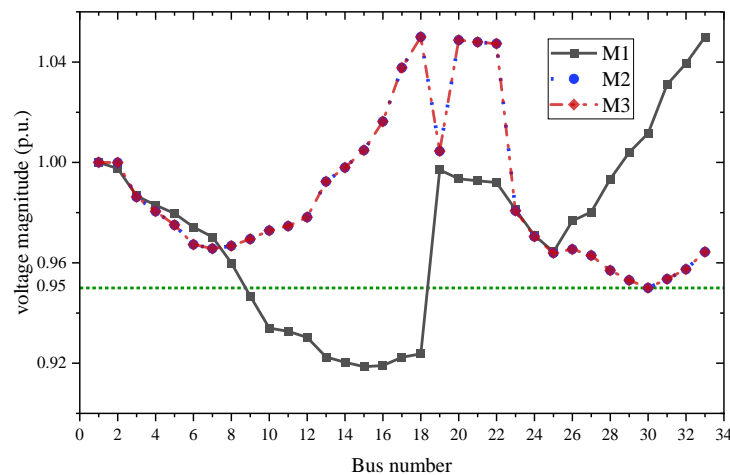


Figure 7. The voltage magnitude in the PDN when EVs penetrate 50%.

It is evident that there is an enhancement in the voltage magnitude, particularly at node 18, for M2 and M3. Additionally, the voltage distribution in the PDNs is effectively maintained. The coordinated strategy uses the charging price for the PDNs to incentivise EVs to charge at specific stations, such as EVCS 1 and 4. Therefore, it can efficiently mitigate traffic congestion and the low voltage problem at distribution network nodes generated by the independent scheme. This guarantees the secure and effective functioning of the power–traffic network.

After conducting a thorough examination of operational costs, EV charging numbers, and voltage magnitude, we evaluated the calculation time of three approaches in two common scenarios, peak and off-peak, to further examine their usefulness. Table 3 clearly demonstrates that M1 has the shortest computation time. Nevertheless, it fails to accomplish the most efficient functioning of the PTNs, which could potentially jeopardise the secure

operating of the PDNs. As M2 approaches its optimal state, it heavily depends on the transmission of large amounts of data between the power and traffic systems. This raises concerns over the privacy of information and the practicality of its implementation. When comparing M2 with M3, it is evident that M3 achieves a better balance between maintaining system privacy and providing precise solutions. Additionally, M3 is able to provide accuracy even when working with little data.

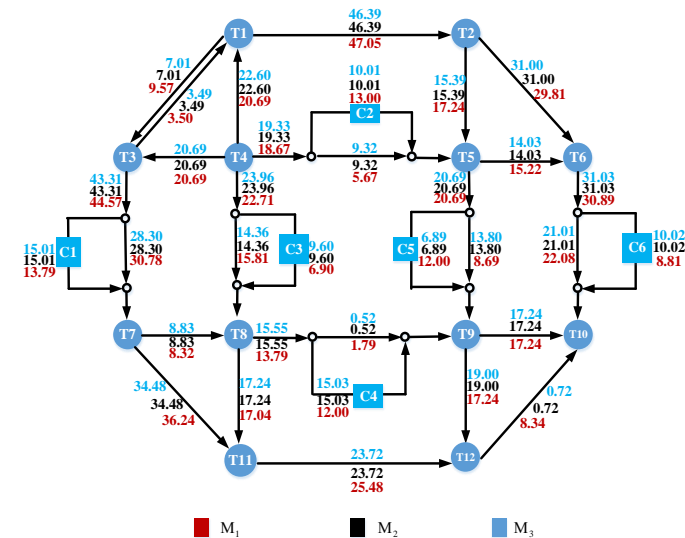


Figure 8. The traffic flow of the UTN when EVs penetrate 50%.

Table 3. Computation times of different methods.

Different EV Penetrations	Time of M ₁ (s)	Time of M ₂ (s)	Time of M ₃ (s)
10%	14.42	46.14	169.34
20%	15.13	47.39	170.05
30%	15.98	49.36	171.96
40%	16.56	50.47	172.56
50%	17.26	52.30	173.31

Figure 8 displays the traffic patterns during peak hours ($t = 10$) in the UTN for in-depth examination. The figure reveals that the majority of vehicles opt to travel on the inner and outer loops due to their higher capacities and fewer traffic signals (t_0) compared to other connections. The traffic flow of the charging link (T4–T5) in the coordinated system is 10.01 p.u., which indicates a 20% reduction compared to the autonomous scheme. The coordinated scheduling strategy considers the secure operation of the PDNs. By modifying the charging fees, voltage losses in the vicinity can be reduced, thereby diverting charging vehicles to other EVCSs. Furthermore, the traffic patterns achieved by M3 are identical to the centralised optimisation of the interconnected PTNs, which is solved by M2. This suggests that the use of boundary information mapping and cost functions can effectively replace the original power grid model with M3. By employing the suggested approach, the correctness of optimisation outcomes for the interconnected PTNs is guaranteed, while also safeguarding the confidentiality of sensitive system information.

5.3. Comparative Analysis of the Case Studies

This section examines the influence of various charging station connection sites on the power–traffic coupling system. Figure 9 illustrates the topology for scenario 2, which is distinct from the topologies shown in Figures 3 and 4. The parameter configurations align with those outlined in Section 5.2.

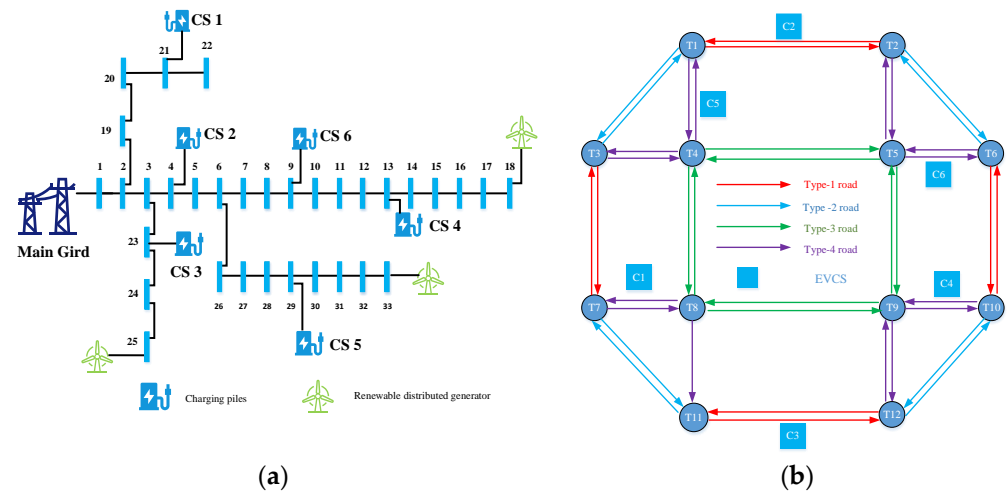


Figure 9. (a) Comparative case topology of the PDN with different charging station connections. (b) Comparative case topology of the UTN with different charging station connections.

Figure 10 displays the overall expenses of the PTNs at various locations. In contrast to instance 1, the bulk of the charging stations are situated within or in close proximity to the outer circle. Figure 10 demonstrates that the overall operational expenses in case 2 are often more than those in case 1. The greater operational costs are caused by the positioning of charging stations along the outer loops and capacity, which forces EVs to detour from the optimal path and travel extra distances to access the charging stations. From these data, it can be inferred that placing charging stations along the outer ring has an adverse effect on the overall operational expenses of the EVs. In order to maximise cost-effectiveness, it is advisable to strategically position charging stations along the inner loop, so minimising any extra trip time.

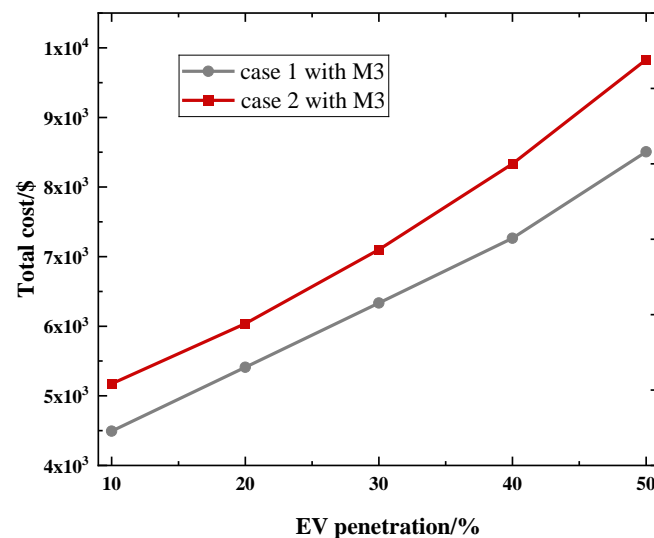


Figure 10. Comparison of total costs under different charging station locations.

Figure 11 illustrates the voltage magnitudes for various charging station sites when the EV penetration rate is 50%. Case 2 exhibits fewer voltage variations compared to case 1. In scenario 1, a substantial quantity of electric vehicles congregate at EVCS 5, which is situated within the inner circle. This efficiently decreases the amount of time spent travelling while still satisfying the need for travel. The voltage near node 30 approaches its limit as a result. In case 2, the charging stations are strategically placed in the outer ring or near the outer

loop. This arrangement helps to decentralise the charging of EVs and minimise the strain on the PDN, resulting in a reduction in voltage fluctuations.

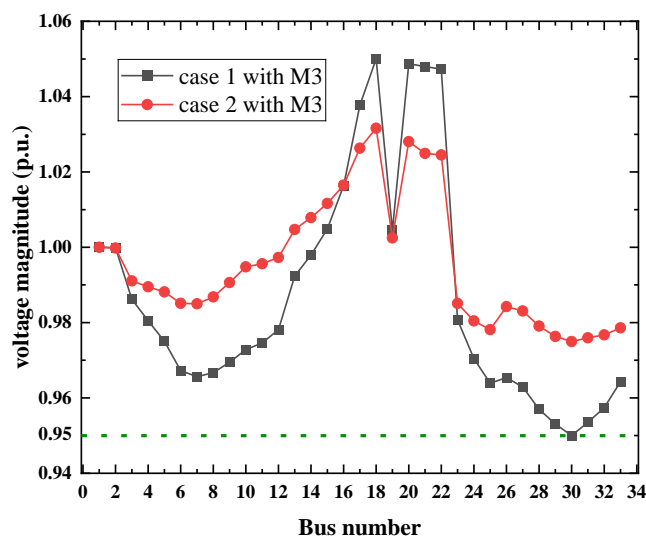


Figure 11. Comparison of voltage magnitudes under different charging station locations.

6. Conclusions

This research introduces a new coordinated scheduling technique for PTNs that addresses the limitations of previous coordinated optimisation methods. The method utilises boundary information mapping and implements a non-iterative framework for the PTNs. Using this proposed approach, the efficient functioning of the PDNs is translated into a mathematical equation and a safety operation set with minimum data, enabling the PDNs to attain external equivalence. The suggested model replaces the PDNs by utilising partial boundary information, allowing for coordinated optimisation of the PTNs. This approach eliminates the need for iterative solutions between the linked systems. By maintaining uniformity in the highest level of effectiveness, it simultaneously ensures confidentiality and protection across many systems. A case analysis is performed on a system that consists of a 12-node traffic network and an IEEE 33-bus system in order to verify the efficacy of the suggested method. The main discoveries are as follows: (1) The proposed method for mapping the feasible domain can effectively align the operational limitations of the power grid, enabling coordinated scheduling of the power–traffic network while safeguarding the confidentiality of power grid information. (2) In comparison to independently scheduling the two networks, the coordinated scheduling of the power–traffic networks can optimise the distribution of electric vehicle traffic flow and charging load in both the power grid and the traffic network, thereby enhancing the safety and efficiency of the power–traffic networks.

Author Contributions: Conceptualization, W.D.; Methodology, W.D.; Software, Z.Z. (Zhihong Zeng); Validation, Z.Z. (Zhihong Zeng); Investigation, Z.Z. (Zhihong Zeng) and J.X.; Resources, C.W.; Data curation, C.W. and Y.G.; Writing—original draft, Z.Z. (Zhihong Zeng); Writing—review & editing, W.D.; Supervision, Z.Z. (Zhijie Zhang); Funding acquisition, W.D. All authors have read and agreed to the published version of the manuscript.

Funding: This research was funded by the National Natural Science Foundation of China under grant No.52107082 and the Specific Research Project of Guangxi for Research Bases and Talents under grant No.AD22080052. The funder is Wei Dai.

Data Availability Statement: The raw data supporting the conclusions of this article will be made available by the authors on request.

Acknowledgments: The authors would like to thank Huihwang Goh for his help in our research. We appreciate the discussions and comments from all of the editors and anonymous reviewers.

Conflicts of Interest: Author Cheng Wang was employed by the Gui'an Power Supply Bureau of Guizhou Power Grid Co., Ltd. The remaining authors declare that the research was conducted in the absence of any commercial or financial relationships that could be construed as a potential conflict of interest.

References

1. Lopes, J.A.P.; Soares, F.J.; Almeida, P.M.R. Integration of Electric Vehicles in the Electric Power System. *Proc. IEEE* **2011**, *99*, 168–183. [CrossRef]
2. Global EV Outlook 2022 [EB/OL]. [Online]. Available online: <https://www.iea.org/reports/global-ev-outlook-2022> (accessed on 25 December 2023).
3. Kezunovic, M.; Waller, S.T.; Damnjanovic, I. Framework for studying emerging policy issues associated with phev's in managing coupled power and transportation systems. In Proceedings of the 2010 IEEE Green Technologies Conference, Grapevine, TX, USA, 15–16 April 2010; pp. 1–8.
4. Yang, W.; Liu, W.; Chung, C.Y.; Wen, F. Joint planning of EV fast charging stations and power distribution systems with balanced traffic flow assignment. *IEEE Trans. Ind. Inform.* **2020**, *17*, 1795–1809.
5. Zhang, H.; Hu, Z.; Song, Y. Power and transport nexus: Routing electric vehicles to promote renewable power integration. *IEEE Trans. Smart Grid* **2020**, *11*, 3291–3301. [CrossRef]
6. Wei, W.; Wu, L.; Wang, J.; Mei, S. Network equilibrium of coupled transportation and power distribution systems. *IEEE Trans. Smart Grid* **2017**, *9*, 6764–6779. [CrossRef]
7. Shi, B.; Dai, W.; Luo, C.; Goh, H.H.; Li, J. Modeling and Impact Analysis for Solar Road Integration in Distribution Networks. *IEEE Trans. Sustain. Energy* **2022**, *14*, 935–947. [CrossRef]
8. Qian, T.; Shao, C.; Li, X.; Wang, X.; Shahidehpour, M. Enhanced coordinated operations of electric power and transportation networks via EV charging services. *IEEE Trans. Smart Grid* **2020**, *11*, 3019–3030. [CrossRef]
9. Sun, Y.; Chen, Z.; Li, Z.; Tian, W.; Shahidehpour, M. EV charging schedule in coupled constrained networks of transportation and power system. *IEEE Trans. Smart Grid* **2018**, *10*, 4706–4716. [CrossRef]
10. Baghali, S.; Guo, Z.; Wei, W.; Shahidehpour, M. Electric Vehicles for Distribution System Load Pickup Under Stressed Conditions: A Network Equilibrium Approach. *IEEE Trans. Power Syst.* **2023**, *38*, 2304–2317. [CrossRef]
11. Guo, Z.; Afifah, F.; Qi, J.; Baghali, S. A stochastic multiagent optimization framework for interdependent transportation and power system analyses. *IEEE Trans. Transp. Electrification* **2021**, *7*, 1088–1098. [CrossRef]
12. Shao, C.; Li, K.; Qian, T.; Shahidehpour, M.; Wang, X. Generalized user equilibrium for coordination of coupled power-transportation network. *IEEE Trans. Smart Grid* **2022**, *14*, 2140–2151. [CrossRef]
13. Sadhu, K.; Haghshenas, K.; Rouhani, M.; Aiello, M. Optimal joint operation of coupled transportation and power distribution urban networks. *Energy Inform.* **2022**, *5*, 35. [CrossRef]
14. Sun, G.; Li, G.; Xia, S.; Shahidehpour, M.; Lu, X.; Chan, K.W. ALADIN-based coordinated operation of power distribution and traffic networks with electric vehicles. *IEEE Trans. Ind. Appl.* **2020**, *56*, 5944–5954. [CrossRef]
15. Liu, J.; Lin, G.; Huang, S.; Zhou, Y.; Rehtanz, C.; Li, Y. Collaborative EV routing and charging scheduling with power distribution and traffic networks interaction. *IEEE Trans. Power Syst.* **2022**, *37*, 3923–3936. [CrossRef]
16. Aghajan-Eshkevari, S.; Ameli, M.T.; Azad, S. Optimal routing and power management of electric vehicles in coupled power distribution and transportation systems. *Appl. Energy* **2023**, *341*, 121126. [CrossRef]
17. Lu, Z.; Xu, X.; Yan, Z.; Shahidehpour, M. Multistage robust optimization of routing and scheduling of mobile energy storage in coupled transportation and power distribution networks. *IEEE Trans. Transp. Electrification* **2021**, *8*, 2583–2594. [CrossRef]
18. Lv, S.; Chen, S.; Wei, Z. Coordinating Urban Power-Traffic Networks: A Subsidy-Based Nash–Stackelberg–Nash Game Model. *IEEE Trans. Ind. Inform.* **2022**, *19*, 1778–1790. [CrossRef]
19. Xie, S.; Xu, Y.; Zheng, X. On dynamic network equilibrium of a coupled power and transportation network. *IEEE Trans. Smart Grid* **2021**, *13*, 1398–1411. [CrossRef]
20. Xie, S.; Wu, Q.; Hatziargyriou, N.D.; Zhang, M.; Zhang, Y.; Xu, Y. Collaborative pricing in a power-transportation coupled network: A variational inequality approach. *IEEE Trans. Power Syst.* **2022**, *38*, 783–795. [CrossRef]
21. Lai, X.; Xie, L.; Xia, Q.; Zhong, H.; Kang, C. Decentralized multi-area economic dispatch via dynamic multiplier-based Lagrangian relaxation. *IEEE Trans. Power Syst.* **2014**, *30*, 3225–3233. [CrossRef]
22. Jiang, H.; Zhang, Y.; Chen, Y.; Zhao, C.; Tan, J. Power-traffic coordinated operation for bi-peak shaving and bi-ramp smoothing—A hierarchical data-driven approach. *Appl. Energy* **2018**, *229*, 756–766. [CrossRef]
23. Xie, S.; Chen, Z.; Zhang, Y.; Cao, S.; Chen, K. Decentralized optimization of multi-area power-transportation coupled systems based on variational inequalities. *CSEE J. Power Energy Syst.* **2023**. *early access*. [CrossRef]
24. Huang, S.; Wu, Q. Dynamic tariff-subsidy method for PV and V2G congestion management in distribution networks. *IEEE Trans. Smart Grid* **2019**, *10*, 5851–5860. [CrossRef]
25. Alizadeh, M.; Wai, H.T.; Chowdhury, M.; Goldsmith, A.; Scaglione, A.; Javidi, T. Optimal pricing to manage electric vehicles in coupled power and transportation networks. *IEEE Trans. Control Netw. Syst.* **2016**, *4*, 863–875. [CrossRef]
26. Zhou, Z.; Liu, Z.; Su, H.; Zhang, L. Integrated pricing strategy for coordinating load levels in coupled power and transportation networks. *Appl. Energy* **2022**, *307*, 118100. [CrossRef]

27. Mouna, K.-B. Charging station location problem: A comprehensive review on models and solution approaches. *Transp. Res. Part C Emerg. Technol.* **2021**, *132*, 103376.
28. Loaiza, Q.C.; Arbelaez, A.; Climent, L. Robust ebuses charging location problem. *IEEE Open J. Intell. Transp. Syst.* **2022**, *3*, 856–871. [[CrossRef](#)]
29. Efthymiou, D.; Chrysostomou, K.; Morfoulaki, M.; Aifantopoulou, G. Electric vehicles charging infrastructure location: A genetic algorithm approach. *Eur. Transp. Res. Rev.* **2017**, *9*, 27.
30. Majhi, R.C.; Ranjitkar, P.; Sheng, M.; Covic, G.A.; Wilson, D.J. A systematic review of charging infrastructure location problem for electric vehicles. *Transp. Rev.* **2021**, *41*, 432–455. [[CrossRef](#)]
31. Burak, K.Ö.; Gzara, F.; Alumur, S.A. Full cover charging station location problem with routing. *Transp. Res. Part B Methodol.* **2021**, *144*, 1–22.
32. Kun, A. Battery electric bus infrastructure planning under demand uncertainty. *Transp. Res. Part C Emerg. Technol.* **2020**, *111*, 572–587.
33. An, Y.; Gao, Y.; Wu, N.; Zhu, J.; Li, H.; Yang, J. Optimal scheduling of electric vehicle charging operations considering real-time traffic condition and travel distance. *Expert Syst. Appl.* **2023**, *213*, 118941. [[CrossRef](#)]
34. Padraigh, J.; Climent, L.; Arbelaez, A. *Smart and Sustainable Scheduling of Charging Events for Electric Buses. EU Cohesion Policy Implementation—Evaluation Challenges Opportunities*; Springer Nature: Berlin/Heidelberg, Germany, 2023; pp. 121–129.
35. Manshadi, S.D.; Khodayar, M.E.; Abdelghany, K.; Üster, H. Wireless charging of electric vehicles in electricity and transportation networks. *IEEE Trans. Smart Grid* **2017**, *9*, 4503–4512. [[CrossRef](#)]
36. Alizadeh, M.; Wai, H.T.; Goldsmith, A.; Scaglione, A. Retail and wholesale electricity pricing considering electric vehicle mobility. *IEEE Trans. Control Netw. Syst.* **2018**, *6*, 249–260. [[CrossRef](#)]
37. Qiao, W.; Han, Y.; Zhao, Q.; Si, F.; Wang, J. A distributed coordination method for coupled traffic-power network equilibrium incorporating behavioral theory. *IEEE Trans. Veh. Technol.* **2022**, *71*, 12588–12601. [[CrossRef](#)]
38. Tao, D.; Bie, Z. Parallel augmented Lagrangian relaxation for dynamic economic dispatch using diagonal quadratic approximation method. *IEEE Trans. Power Syst.* **2016**, *32*, 1115–1126.
39. Benders, J.F. Partitioning procedures for solving mixed-variables programming problems. *Comput. Manag. Sci.* **2005**, *2*, 3–19. [[CrossRef](#)]
40. Li, Z.; Wu, W.; Zhang, B.; Wang, B. Decentralized multi-area dynamic economic dispatch using modified generalized benders decomposition. *IEEE Trans. Power Syst.* **2015**, *31*, 526–538. [[CrossRef](#)]
41. Lin, C.; Wu, W. A nested decomposition method and its application for coordinated operation of hierarchical electrical power grids. *arXiv* **2020**, arXiv:2007.02214.
42. Tan, Z.; Yan, Z.; Zhong, H.; Xia, Q. Non-Iterative Solution for Coordinated Optimal Dispatch via Equivalent Projection—Part II: Method and Applications. *IEEE Trans. Power Syst.* **2023**, *39*, 899–908. [[CrossRef](#)]
43. Tan, Z.; Yan, Z.; Zhong, H.; Xia, Q. Non-Iterative Solution for Coordinated Optimal Dispatch via Equivalent Projection—Part I: Theory. *IEEE Trans. Power Syst.* **2024**, *39*, 890–898. [[CrossRef](#)]
44. Dai, W.; Wang, C.; Goh, H.; Zhao, J.; Jian, J. Hosting Capacity Evaluation Method for Power Distribution Networks Integrated with Electric Vehicles. *J. Mod. Power Syst. Clean Energy* **2023**, *11*, 1564–1575. [[CrossRef](#)]
45. Bolognani, S.; Zampieri, S. On the existence and linear approximation of the power flow solution in power distribution networks. *IEEE Trans. Power Syst.* **2015**, *31*, 163–172. [[CrossRef](#)]
46. Yang, J.; Zhang, N.; Kang, C.; Xia, Q. A state-independent linear power flow model with accurate estimation of voltage magnitude. *IEEE Trans. Power Syst.* **2016**, *32*, 3607–3617. [[CrossRef](#)]

Disclaimer/Publisher’s Note: The statements, opinions and data contained in all publications are solely those of the individual author(s) and contributor(s) and not of MDPI and/or the editor(s). MDPI and/or the editor(s) disclaim responsibility for any injury to people or property resulting from any ideas, methods, instructions or products referred to in the content.